Evidence for nuclear molecular orbital effects in the $^{13}C+^{13}C \rightarrow ^{12}C+^{14}C$ transfer reaction

S. K. Korotky,* K. A. Erb,† R. L. Phillips,‡ S. J. Willett,§ and D. A. Bromley
A. W. Wright Nuclear Structure Laboratory, Yale University, New Haven, Connecticut 06511
(Received 28 February 1983)

Detailed measurements of the angular distribution for the $^{13}C+^{13}C \rightarrow ^{12}C+^{14}C$ single neutron transfer reaction as a function of bombarding energy from just above the Coulomb barrier to approximately four times the barrier energy are reported. The distorted-wave Born approximation for the transfer process does not reproduce the strong oscillations observed in both the experimental angular distributions and excitation functions, while analyses using a two-pole model for the transfer amplitude indicate significant multistep contributions. We show that the cross section in the 90° region in the center of mass is characteristic of an increased collision delay time and of an effective Q value 1 MeV smaller than the asymptotic observable Q value. Angular distributions calculated using the dynamic two-center shell model of Konnecke *et al.* also succeed in reproducing the salient features of the data. The present experiment provides evidence for the occurrence of single-particle nuclear molecular behavior in a heavy-ion neutron transfer reaction. Data for the elastic scattering of $^{13}C+^{13}C$ are also presented and analyzed. We conclude that the elastic scattering excitation functions are consistent with the occurrence of orbiting in the dynamic interaction.

[NUCLEAR REACTIONS $^{13}C(^{13}C,^{12}C)^{14}C$ and $^{13}C(^{13}C,^{14}C)^{12}C$, measured $\sigma(E;\theta)$, $E(\text{lab})=16.0$–50.0 MeV, $\theta(\text{lab})=17.8°$–$51.4°$, comparison with DWBA calculations, analysis using two-pole model, interpreted as evidence for reduced effective Q value in the surface region and an increase in the collision delay time compared to values expected for a single step process; $^{13}C(^{13}C,^{13}C)^{13}C$, measured $\sigma(E)$, $\theta(\text{lab})=25°$, 30°, 35°, 40°, 45°, $E(\text{lab})=14.5$–71.0 MeV, optical model calculations, analysis using one pole model, gross structure oscillations interpreted as a geometrical effect.]

I. INTRODUCTION

The nature of the process of nucleon transfer in heavy-ion collisions is not fully understood. In some cases the distorted-wave Born approximation (DWBA) provides an adequate representation of the experimental observations, while in other cases there are significant discrepancies.[1–4] It has been proposed by several authors that single-particle molecular orbital (MO) effects may play an important role in the transfer process and would resolve the apparent discrepancies.[5–9] Such effects would include, for example, the distortion (or polarization) of the wave function describing the motion of the transferred nucleon from its asymptotic form and a corresponding shift in the internal energy when the colliding nuclei are in proximity. The occurrence of these effects would imply that there is a time interval during the reaction when the motion of the transferred nucleon is strongly and simultaneously influenced by both the nucleus to which it was initially bound, and the nucleus encountered during the collision. This behavior, analogous to atomic molecular motion, is of intrinsic interest.

Von Oertzen *et al.*[10] have presented evidence for molecular orbital behavior in the elastic scattering of $^{12}C+^{13}C$. However, to date, no unambiguous evidence of nuclear single-particle MO behavior in a nucleon transfer reaction has been established. In this paper we report the results of experiments to investigate the angle and energy dependence of the cross section for a neutron transfer reaction considered to be a good candidate for the occurrence and observation of MO effects. We have found that the DWBA does not reproduce the salient features of the data. Using a two-pole model for the transfer amplitude, the systematics of the data can be understood as arising from a shift in the internal energy during the scattering process and an increase in the collision delay time over that value expected for a single-step (DWBA) process. Our findings suggest that single-particle molecular orbital behavior may play an important role in the nuclear reaction dynamics.

We chose to investigate the $^{13}C+^{13}C \rightarrow ^{12}C+^{14}C$ reaction for evidence of MO behavior. Spin-averaged angular distributions for the ground state to ground state transition were measured at eighteen energies in the region extending from just above the Coulomb barrier to approximately four times the barrier energy, i.e., $16.0 \leq E_{\text{lab}} \leq 50.0$ MeV. This range was studied because at these energies the transfer reaction is not dominated merely by barrier penetration, and, in addition, the energy is not so large that the collision time can be considered negligible compared to the internal rearrangement time. We have also measured excitation functions for $^{13}C+^{13}C$ elastic scattering to provide information concerning the relative motion potentials. This paper is the more thorough description of the experimental work and analyses previously summarized.[11]

II. EXPERIMENTAL METHOD

A. Particle beam and targets

Common to all of the experiments described here were the ^{13}C particle beam and ^{13}C targets. The carbon-13 beam was obtained by directly extracting ^{13}C negative ions from a UNIS sputter source fitted with an enriched (90%) ^{13}C cone and accelerating the ions to 15—71 MeV using the MP tandem Van de Graaff accelerator of this laboratory. Before striking the target the beam was momentum analyzed and had an estimated energy spread of approximately 15 keV. The beam spot size ($\simeq$1.5 mm), angle of incidence, and angle of divergence of the beam at the target contributed less than 0.15° to the angular resolution of the experiments. Beam currents were chosen in the range of 10 to 400 nA so that, depending on beam energy and detector angle, electronic dead time was limited to less than six percent.

The targets consisted of isotopically enriched (97%) self-supporting ^{13}C foils having a nominal thickness of 30 $\mu g/cm^2$. This thickness results in an effective loss in beam energy of approximately 80 keV at the lowest energies (=30 keV at the highest), and increases the average upper limit for the energy uncertainty about the mean energy to about $\pm$60 keV when straggling is also accounted for. Besides the desired ^{13}C component, the targets contained observable amounts of carbon-12 and oxygen-16 contaminants. To eliminate possible background contributions from these contaminants, we used kinematic coincidence techniques in obtaining the elastic scattering and transfer reaction cross sections.

B. Elastic scattering measurements

The detection apparatus for the $^{13}C+^{13}C$ elastic scattering measurements consisted of pairs of large area (1 cm$\times$ 5 cm) silicon surface barrier detectors. The detectors of a given pair were placed on opposite sides of the beam axis, separated by an angle of 90° in the reaction plane, and were operated in slow time coincidence ($\Delta t \leq 1$ μs). Data were collected simultaneously at five angles by using five pairs of detectors.

One detector from each pair was used to form a group of five defining detectors. The detectors of the defining group had arc-shaped polar angle apertures of 0.3° and an average solid angle of 0.8×10^{-3} sr. After accounting for beam definition effects, the estimated total angular resolution of the experiments is still better than 0.5°. The defining detectors were placed at angles corresponding to the center of mass angles of 50°, 60°, 70°, 80°, and 90°. The placement of each detector was determined to within 0.1° of the aperture defined beam direction. The scattering angle was verified by the observed symmetry of the cross section about $\theta=90°$ in the center of mass. To ensure complete detection efficiency for $^{13}C+^{13}C$ elastic scattering events, and yet reject events corresponding to $^{12}C+^{13}C$ elastic scattering, the angular apertures of the detectors constituting the coincidence group were chosen to be approximately 1° wide and to subtend a substantially greater out of plane angle than the defining slits.

Using the detector array described above, $^{13}C+^{13}C$ elastic scattering differential cross sections for five angles were measured at 1 MeV energy increments (lab) from $E_{beam}=14.5$ to 71.0 MeV. Relative energy to energy cross sections were obtained by correcting the laboratory particle yields for integrated beam current (including average beam charge state correction), and electronic dead time. Angle-to-angle normalization was accomplished by rotating the system of detectors and making overlap measurements. The results were consistent with the geometrical solid angle ratios. Absolute normalization of the data, as well as an independent consistency check on the angle to angle normalization, were obtained by matching the 70°, 80°, and 90° excitation functions with previous measurements of $^{13}C+^{13}C$ angular distributions made by our group in the region of the Coulomb barrier.[12] These normalizations are supported by the observation that the cross sections for the more forward angles (50° and 60°) at the lowest energies are close to the calculated Mott values.

The experimental $^{13}C+^{13}C$ elastic scattering excitation functions are plotted in Fig. 1. The data are shown as ratios to the Mott scattering cross section in order to remove some of the average energy dependence and to display more clearly the effects of the nuclear interaction. We note that the calculated oscillations in the energy dependence of the symmetrized Coulomb cross sections have longer periods and smaller amplitudes than those observed in the experimental excitation functions, and that the gross structure oscillations evident in this figure are indeed of nuclear origin. The errors illustrated in Fig. 1 are predominantly statistical; the uncertainty in absolute normalization is approximately five percent. For completeness, the data from our previous experiment, which largely determined the absolute normalization factor for the present experiment, are also plotted (70°, 80°, 90°; $5 \leq E_{c.m.} \leq 7.5$ MeV). We note that our values for the 60° excitation function are in excellent agreement with those measured by Helb *et al.*[13] in the range $7 \leq E_{c.m.} \leq 12$ MeV. Our relative 90° cross sections are also in good agreement with theirs in the energy range studied; however, our absolute 90° cross sections are nearly two times larger. We have been unable to explain this as a discrepancy arising from a systematic error in the present experiment and we attribute it to a difference in the technique used to remove $^{12}C+^{13}C$ elastic scattering background, which can be significant in the 90° region.

C. Neutron transfer measurements

To measure the cross section for the $^{13}C+^{13}C \rightarrow ^{12}C+^{14}C$ reaction over a wide energy and angular region efficiently and to use the kinematic coincidence method to identify events, we replaced the multiple pairs of standard solid state detectors used for the elastic scattering measurements with a single pair of large area (1 cm$\times$5cm) position sensitive detectors (PSD's). These PSD's were silicon surface barrier detectors with approximately 1% position resolution along their length. The defining and coincident PSD's were positioned on opposite sides of the beam 15.2 cm and 13.4 cm from the target, respectively. We masked the defining and coincident PSD's to subtend polar angles of approximately 14° and 20°, respectively, while in the azimuthal direction the pair of detectors was collimated to 4° located symmetrically about the horizontal reaction plane. To obtain an-

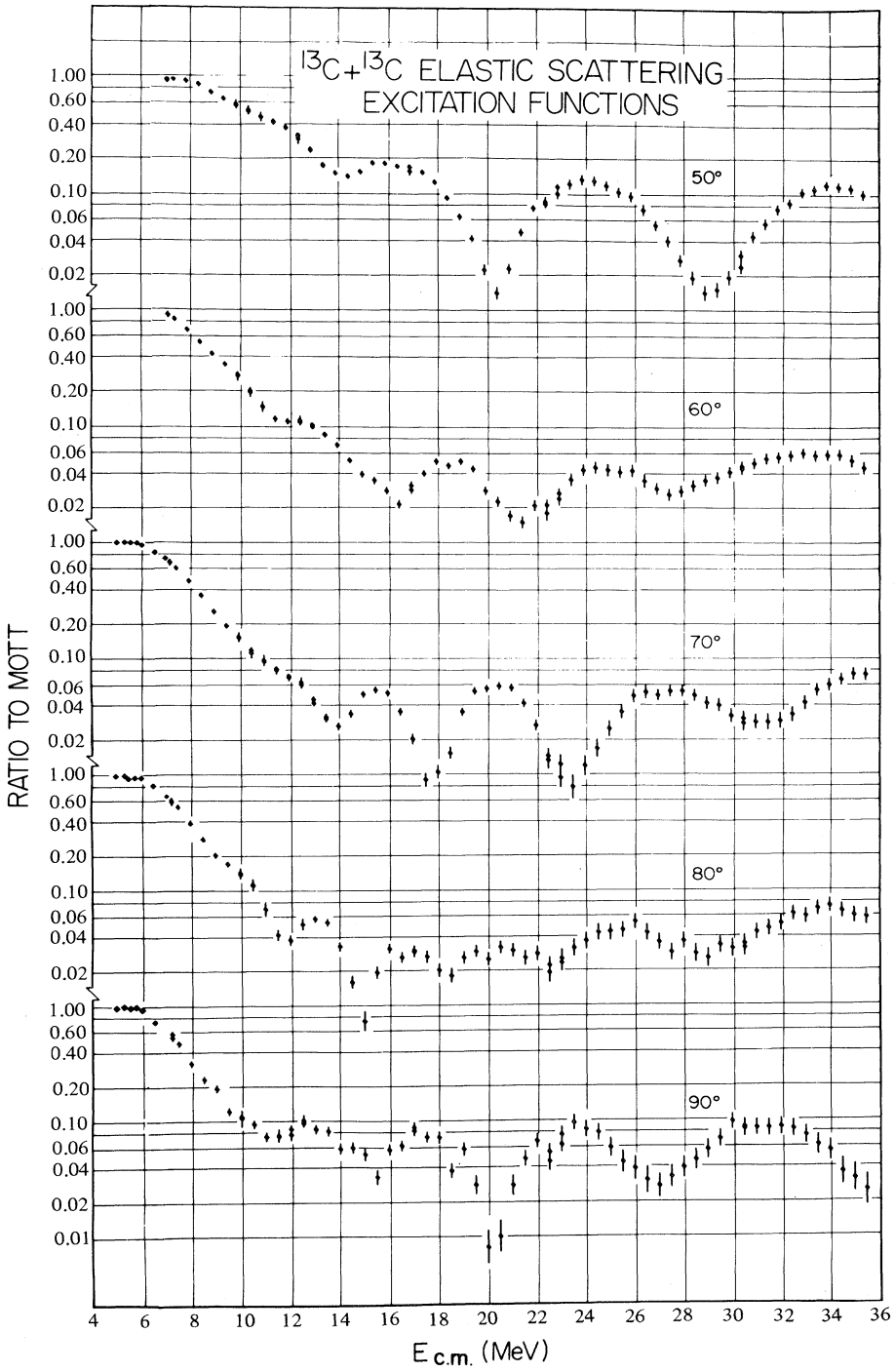

FIG. 1. Experimental $^{13}C+^{13}C$ elastic scattering excitation functions.

gle and solid angle definition, a machined mask consisting of fifteen rectangular apertures was situated in front of the defining detector aperture. This provided an angular acceptance of approximately 0.25° per slit and a slit separation of approximately 1.0°. The corresponding solid angle per slit was approximately 0.1×10^{-3} sr.

The combined effects of the finite detector aperture and beam definition yield an angular resolution of the transfer reaction experiments of better than 0.5°. Because the slits were machined as a single unit, the possible error in separation between the slits, and thus in the correspondingly defined angles, was less than 0.02°. The absolute an-

gle of the entire array was determined to within 0.1° by optical alignment. This setting was also verified by the observed symmetry of the transfer reaction angular distribution about $\theta=90°$ in the center of mass.

The positioning of the centers of the defining and coincidence PSD's, θ_d and θ_c, was determined by examining the kinematics for the reactions of interest at several energies in the interval to be studied. An optimized configuration (θ_d,θ_c) was chosen by noting the behavior of the angle of separation $\theta_d+\theta_c$ for the transfer reaction as a function of beam energy, scattering angle (θ_d), and nucleus detected. The configuration was also required to intercept a portion of the elastic scattering kinematics to provide a means of normalizing the transfer data. To cover the desired angular range, three pairs of settings of the PSD's were used: (1) $\theta_d=24.0°$, $\theta_c=74.0°$; (2) $\theta_d=34.5°$, $\theta_c=64.0°$; and (3) $\theta_d=44.0°$, $\theta_c=53.0°$. For each of the three angular settings of the PSD's, measurements of the differential cross section for neutron transfer were made as a function of energy in the interval $E_{\text{beam}}=16.0$ to 50.0 MeV. Because the detection of ^{12}C and ^{14}C at a given laboratory angle corresponds to different center of mass angles for the $^{13}C+^{13}C\rightarrow^{12}C+^{14}C$ reaction, 30 distinct points were obtained for each angular setting of the PSD's giving a total of 90 data points per typical angular distribution.

For the transfer reaction measurements the two PSD's were operated in fast time coincidence ($\Delta t\leq 15$ ns) and the energy and position signals from both were routed to an on-line computer for analysis. To identify uniquely those events corresponding to the $^{13}C(^{13}C,^{13}C)^{14}C$ and $^{13}C(^{13}C,^{14}C)^{12}C$ reactions, the four pieces of kinematic information (two energies, E_c and E_d, and two positions, X_c and X_d) were required to satisfy a series of appropriate pairwise correlations. The correlations tested were E_c versus E_d, E_d versus X_d, and X_c versus X_d. Using the energy-energy correlation, events corresponding to the $^{13}C+^{13}C\rightarrow^{12}C+^{14}C$ neutron transfer to the ground state were easily separated from elastic and inelastic scattering events (in particular, ^{13}C scattering from ^{16}O contamination) because the transfer reaction has a relatively large positive Q value ($Q=+3.23$ MeV). Events corresponding to $^{13}C(^{13}C,^{12}C)^{14}C$ were separated from those corresponding to $^{13}C(^{13}C,^{14}C)^{12}C$ by examining the energy-position and position-position correlations.

For each of the three settings of the PSD's, the yields were corrected for integrated beam current (including average beam charge state effects), electronic dead time, and the relative solid angles of the apertures. These laboratory yields were then converted to relative center of mass cross sections. To match the three angular distribution subsets, we determined the best single normalizing constant (averaged over all energies) for each of the two angular regions where the measurements overlap. The absolute normalization for the entire transfer data set was established by extracting $^{13}C+^{13}C$ elastic scattering yields from the PSD-PSD data at the lower energies and more forward angles, where $^{12}C+^{13}C$ elastic scattering contamination is smallest, and comparing them with our measured elastic scattering excitation functions, which were normalized to the theoretical Mott cross sections for indistinguishable spin-$\frac{1}{2}$ fermions as discussed above.

Figure 2 shows an experimental $^{13}C+^{13}C\rightarrow^{12}C+^{14}C$ angular distribution for a representative energy. Note that six different data point symbols are used in the figure. These correspond to the three settings of the PSD's used and the detection of either ^{12}C or ^{14}C. The continuity of the data over the entire angular region demonstrates the validity of the normalization procedure. We note that the center of mass angles corresponding to the detection of ^{12}C and ^{14}C at the same laboratory angle differ by approximately five degrees. Thus the continuity of the curves provides additional evidence that the reactions were properly identified. Further support for the reaction identification is provided by the observed symmetry about $\theta_{\text{c.m.}}=90°$ that is required for the identical particles in the entrance channel.

The entire PSD-PSD transfer data set is displayed in Fig. 3. In addition to the dominant statistical contribution, the error bars of Fig. 3 include an estimated uncertainty of 1—2% in the integrated beam current and charge state correction factors, and $\leq 4\%$ for the relative normalization factors. The absolute cross section scale has an associated error of $\simeq 10\%$.

To provide a composite view of the measured cross sections, Fig. 4 shows an energy-angle cross section surface plot generated from the experimental data. The curves in Fig. 4 were produced by fitting smooth curves through the experimental angular distributions and extracting the differential cross section at 1° intervals. These condensed data were then energy interpolated to obtain angular distributions in 250 keV increments.

One striking feature of these data is the strong angular oscillations which are present at all energies and which extend to the most forward angle measured. Their presence suggests that the reaction is dominated by a single 1 transfer. The successive increase of the angular momentum of the dominant partial wave with increasing bombarding energy is also apparent in Fig. 4. A phase shift

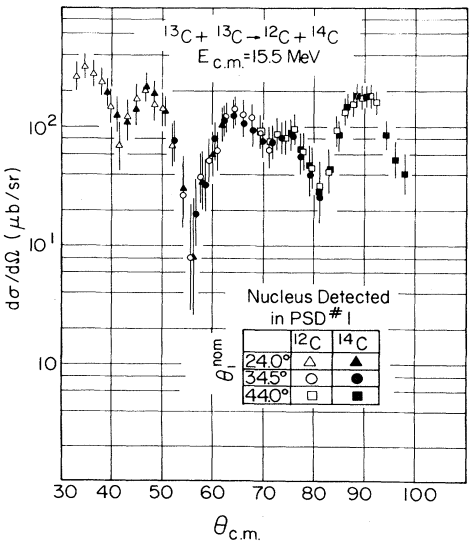

FIG. 2. Representative experimental $^{13}C+^{13}C\rightarrow^{12}C+^{14}C$ (c.m.) angular distribution.

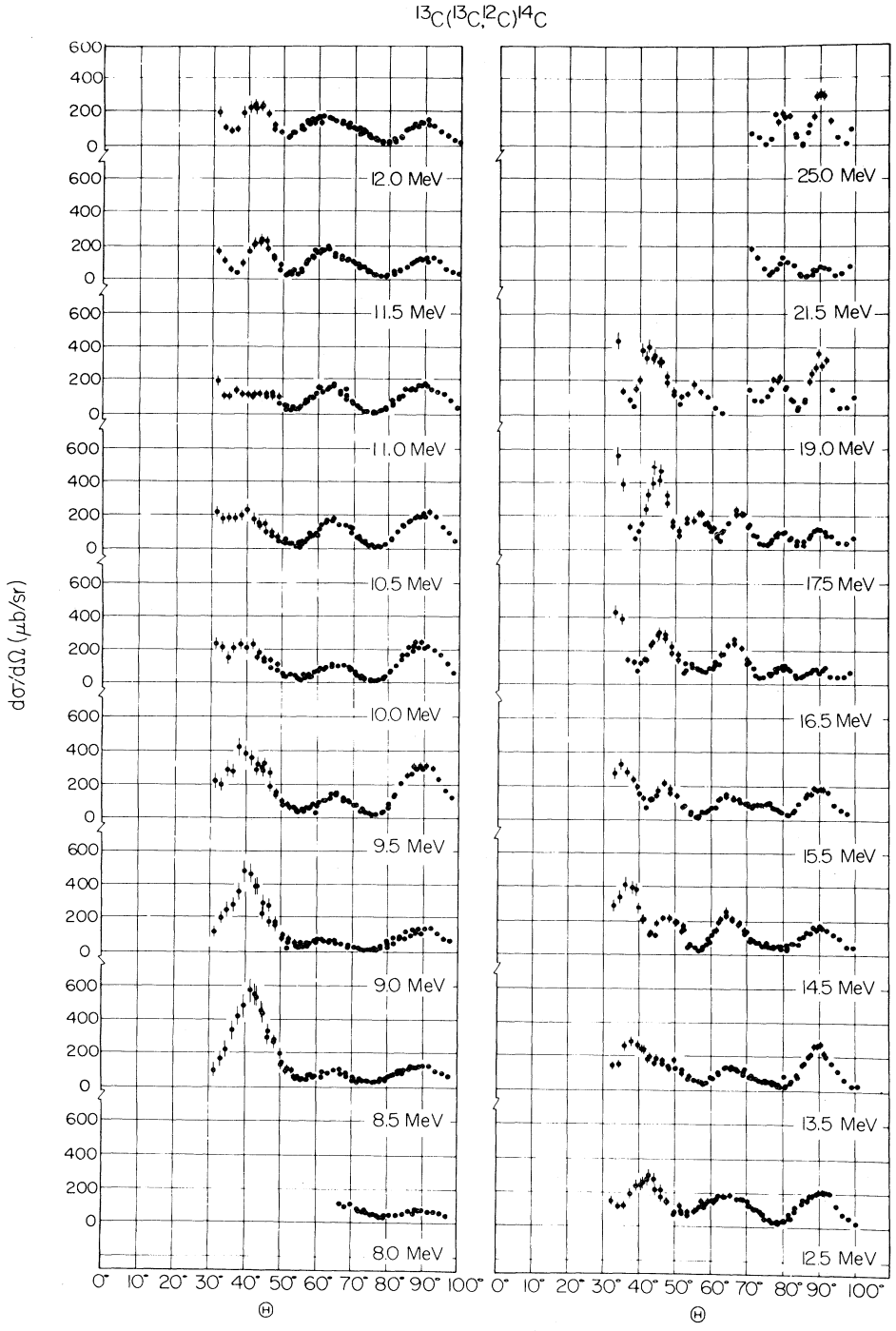

FIG. 3. Complete $^{13}C+^{13}C\rightarrow^{12}C+^{14}C$ angular distribution data set.

analysis of the angular distributions indicates that the dominant partial wave at $E_{c.m.}=19.0$ MeV is about $L=14\hbar$, while at $E_{c.m.}=8.5$ MeV the most important contribution is from $L=8\hbar$.

The change in line density as one follows the ridges of the cross section surface near $\theta_{c.m.}=40°$, 65°, and 90° indicates the excitation functions also show marked structure. This is made explicit in Fig. 5 where the measured 40°, 65°, and 90° excitation functions are plotted. Peak to valley ratios of greater than two to one are common, a feature similar to that observed in heavy-ion elastic and inelastic scattering data. At 90° the peak to valley ratios are greater than 3 to 1, and equally important is the fact that the cross section at the peaks is nearly constant

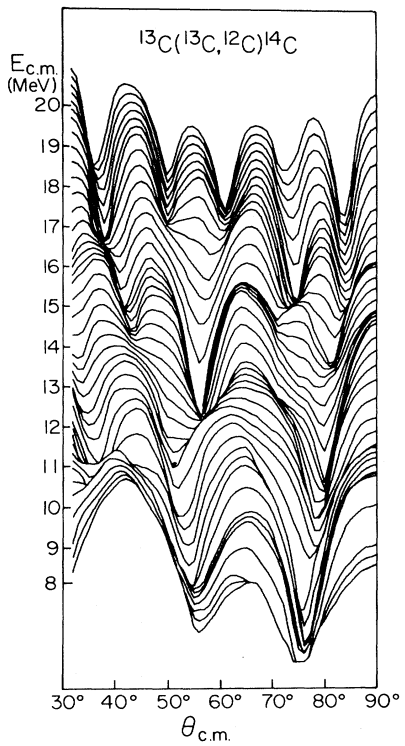

FIG. 4. Energy-angle differential cross section surface for the $^{13}C+^{13}C \rightarrow ^{12}C+^{14}C$ reaction.

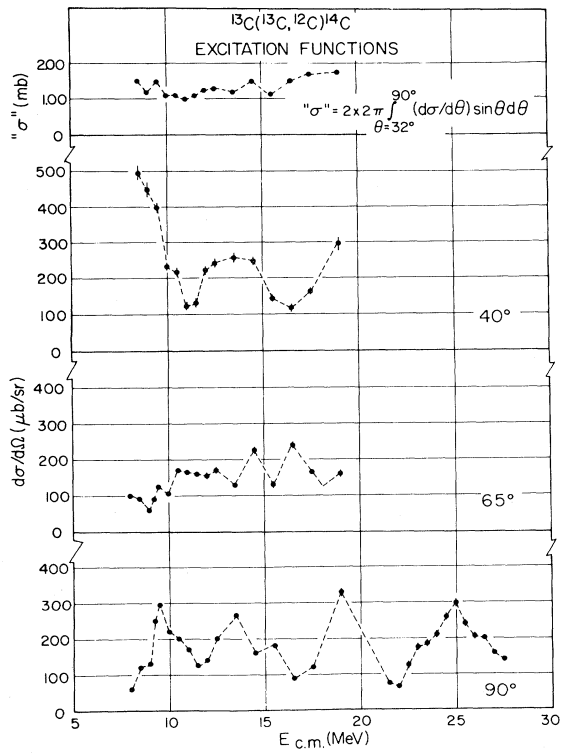

FIG. 5. Experimental $^{13}C+^{13}C \rightarrow ^{12}C+^{14}C$ (g.s.) 90° excitation function.

(300 μb/sr) as a function of energy. As we will discuss below, the calculated DWBA prediction does not agree with this observation.

Figure 5 also displays the angle integrated transfer cross section as a function of energy. The mean value is ~ 1.5 mb with fluctuations at the 25% level, well outside the statistical uncertainty in the integrated yields. A phase shift analysis suggests that the remaining forward angle sector ($0° \leq \theta \leq 32°$), for which no data have been measured, will contribute approximately another 0.5 mb to the total cross section.

III. THE ELASTIC SCATTERING OF $^{13}C+^{13}C$

A. Systematics of the experimental data

To study the systematic features of the $^{13}C+^{13}C$ elastic scattering data we have compared them to some available data for other systems in this mass region. Because analyses of heavy-ion elastic scattering to date indicate that the dominant component of the effective interaction is spin independent, we have chosen the differential cross section at $\theta_{c.m.}=90°$ as the basis for the comparisons. At this angle only even values of the orbital angular momentum contribute regardless of the spin statistics because

$$P_{L=\text{odd}}[\cos(\pi/2)]=0 .$$

Figures 6 and 7 show the experimental 90° excitation function for $^{13}C+^{13}C$ together with the corresponding data for several other systems.[14–18]

When we examine the figures and consider that the various systems are characterized by different spatial sizes, proportional to $(A_1^{1/3}+A_2^{1/3})$, and different charge products, Z_1Z_2, we realize that the gross structure (i.e., features remaining after averaging over energy intervals of ~ 2 MeV) is remarkably similar. The $^{12}C+^{13}C$ system also shows structure which is apparently a common feature of the elastic scattering in this mass region.

The fact that the average magnitudes of the cross sections are not too different suggests that the general absorptive properties in the different systems are similar. In fact, although the fragmentation of the gross structure into components of narrower width obviously calls attention to the uniqueness of the $^{12}C+^{12}C$ system, measurements of the total reaction cross section by our group[19] show that there are no anomalies in the average absorptive properties of this system. It thus appears that the gross structure is closely related to the geometrical properties of the colliding nuclei and is relatively insensitive to differences in the microscopic nuclear structure. The gross structure oscillations described above also occur for the system of closed shell oxygen nuclei ($^{16}O+^{16}O$); consequently, this phenomenon is not believed to be related to an elastic exchange process. These considerations have led us to treat the $^{13}C+^{13}C$ excitation functions in terms of the standard optical model.

B. Optical model calculations

In the DWBA for rearrangement reactions, the relative motion potentials that determine the distorted waves in the entrance and exit channels are usually those that best

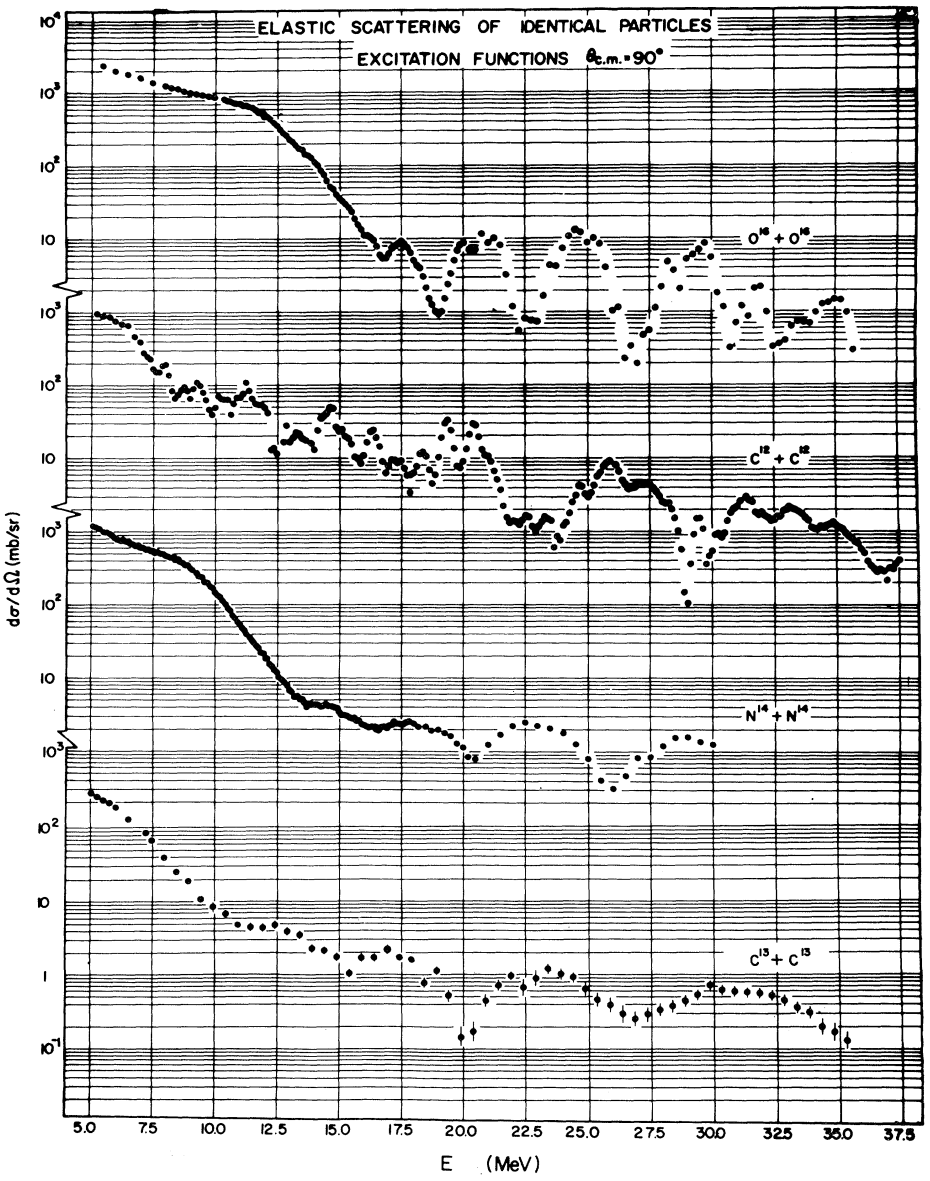

FIG. 6. Comparison of $^{13}C+^{13}C$ 90° elastic excitation function to data for light heavy-ion identical boson systems.

describe the elastic scattering in the corresponding channels. In general, MO models for a given nonelastic reaction predict a modification of the relative motion potentials even in the absence of explicit channel couplings. Thus, the first step in evaluating whether or not the DWBA is a viable model for the transfer reaction under investigation is to determine phenomenological effective potentials which provide a satisfactory representation of $^{13}C+^{13}C$ and $^{12}C+^{14}C$ elastic scattering. Potentials that have been used to describe the average behavior of $^{13}C+^{13}C$ and $^{12}C+^{14}C$ elastic scattering to date have been tested only over a relatively restricted range of energies near the Coulomb barrier.[13,17] Consequently, as part of the present study we have sought to construct a potential that provides a good description of $^{13}C+^{13}C$ and $^{12}C+^{14}C$ elastic scattering over the entire energy interval of present interest.

We have argued above that the general features of the $^{13}C+^{13}C$ 90° excitation function are very similar to those of $^{12}C+^{12}C$ (energy averaged), $^{14}N+^{14}N$, and $^{16}O+^{16}O$ elastic scattering data and that the available $^{12}C+^{13}C$ elastic scattering data fit into the same pattern. Because the behavior of the data for all of these systems is similar, the gross structure can presumably be described by the optical potential. We have performed an extensive search to determine the parameters of a Woods-Saxon optical potential which provides the best description of the $^{13}C+^{13}C$ elastic scattering excitation functions that we have measured.

The calculations were carried out using the computer

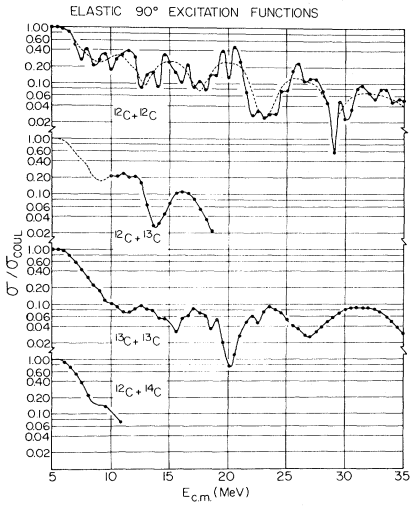

FIG. 7. Comparison of 90° elastic excitation functions for systems of carbon isotopes.

code ATHREE.[20] We considered two classes of potentials distinguished by whether the real part of the nuclear potential was relatively shallow ($V_0 \approx 16$ MeV) or deep ($V_0 \approx 100$ MeV). By adjusting the remaining potential parameters ($r_{0r}, a_r; W_0, r_{0i}, a_i$), it was found that both classes of potentials could describe the data adequately. This lack of sensitivity to the value of the potential for small separation distances presumably reflects strong absorption effects, but we note that sufficient surface transparency is required to reproduce the gross structure oscillations. If the region of strong absorption extended to radii larger than that at which the maximum in the real potential occurred, the calculated structure was strongly damped.

Although this inherent ambiguity in the real potential strength was apparent, we found it considerably easier to control the fitting process using a shallower potential. Thus, for practical purposes we chose to fine tune the parameters of this shallower potential and use it in subsequent calculations. The parameters which provided the best reproduction of the five $^{13}C+^{13}C$ excitation functions shown in Fig. 8 are

$$V_0 = 16.0\ ,\quad r_{0r} = 1.35\ ,\quad a_r = 0.45\ ,$$

$$W_0 = 0.22 \times E_{\text{c.m.}}\ ,\quad r_{0i} = 1.35\ ,\quad a_i = 0.30\ .$$

The agreement with the data represents a significant improvement over those potentials for which the ratio of the imaginary strength to the real strength in the surface region is larger. For each angle the magnitude and oscillatory behavior of the cross section are well reproduced, and, generally speaking, the positions of the maxima and minima are correct. Disagreement with the measurements is most pronounced at 80° where the actual oscillations are somewhat more compressed in the range $10 \leq E_{\text{c.m.}} \leq 30$ MeV than those of the model. The model correctly describes the deviation from Mott scattering as the energy is increased just above the Coulomb barrier.

To place this parameter set into context, it is compared

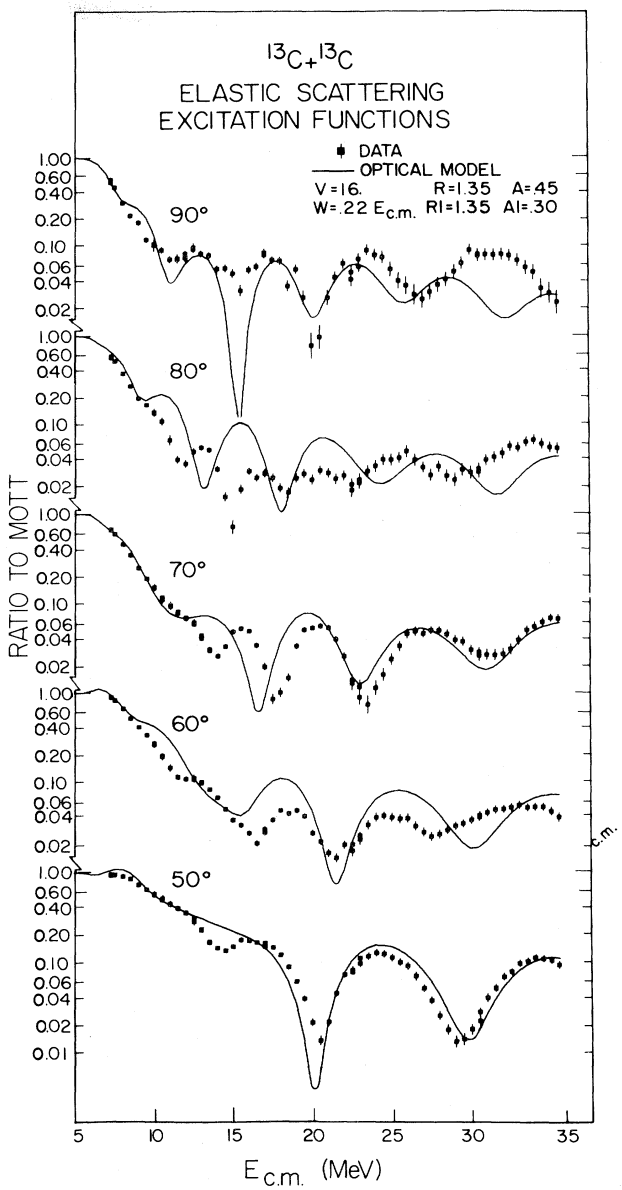

FIG. 8. Optical model calculations and experimental data for $^{13}C+^{13}C$ elastic scattering.

to elastic scattering potentials for other identical particle systems of similar mass in Table I. The parameter sets are qualitatively similar, which is consistent with the similarities observed in the experimental data. Although the systems have intrinsically different sizes and charge products, and hence differing phases and periods of oscillations in the excitation functions, the parameters of the real potential are almost identical after the $A_1^{1/3}+A_2^{1/3}$ factor is removed from the radius. This is a good indication that geometrical aspects, resulting from strong absorption within the barrier, dominate. This also suggests that the optical potential that would best describe $^{12}C+^{14}C$ elastic scattering in model calculations should not be radically different from the potentials used to describe $^{13}C+^{13}C$ elastic scattering.

TABLE I. Comparison of optical parameters for identical light heavy-ion systems.

System	V_0 (MeV)	r_{0r} (fm)	a_r (fm)	W_0 (MeV)	r_{0i} (fm)	a_i (fm)	Ref.
$^{12}C+^{12}C$	14.0	1.35	0.35	$0.4+0.1\times E_{c.m.}$	1.40	0.35	15
$^{13}C+^{13}C$	16.0	1.35	0.45	$0.22\times E_{c.m.}$	1.35	0.30	This work
$^{14}N+^{14}N$	15.0	1.35	0.49	$0.4+0.125\times E_{c.m.}$	1.35	0.49	14
$^{16}O+^{16}O$	17.0	1.35	0.49	$0.4+0.1\times E_{c.m.}$	1.35	0.49	16
$^{16}O+^{16}O$	17.0	1.35	0.49	$0.8+0.1\times E_{c.m.}$	1.27	0.15	21(b)

The characteristics of surface transparency and strong absorption within the barrier are apparently common to all of the systems. This type of potential is necessary to obtain the oscillatory gross structure and also maintain the magnitude of the cross section over the wide energy range. A number of authors[16,21] have studied in detail the properties of the scattering by shallow surface transparent potentials in the case of $^{16}O+^{16}O$ elastic scattering. For example, Gobbi *et al.* were able to correlate the positions of the maxima and minima of the 90° excitation function with the energy regions where the S-matrix elements of even partial waves are near unity and very small, respectively. Assuming that the surface transparent potential is the best representation of the data, they concluded that orbiting probably occurs in $^{16}O+^{16}O$ scattering. We demonstrate in the next section that our results constitute evidence that orbiting also occurs in the $^{13}C+^{13}C$ system.

C. Interpretation of gross structure oscillations

An interpretation of the origin of the elastic scattering gross structure can be obtained from the barrier top model.[22] As discussed by Friedman and Goebel,[23] this model basically depends upon the following assumptions. For each value of the orbital angular momentum L we consider the real potential that is generated by the sum of Coulomb, nuclear (optical), and centrifugal potentials. We assume that the heavy-ion interaction is strongly absorbing inside some radius which is interior to the barrier of the total real potential. The scattering should not be sensitive to the real interaction inside the strong absorption region, and so the major feature of the real potential is the barrier.

In the spirit of obtaining an analytic expression for the elastic S-matrix elements, the model approximates the potential barrier by an inverted parabola. The width, height, and radial position of the inverted parabola, for each value of L, are chosen to duplicate the total real potential near the top of the barrier. Analytical solutions to the Schrödinger equation can then be obtained for the various regions of radial separation: interior to, at, and exterior to the barrier. To obtain the complete solution, the total wave function is required to satisfy the appropriate boundary and matching conditions. In the asymptotic region the incoming flux is normalized to unity, while the outgoing flux is represented by the total reflection coefficient R_L (or, equivalently, the square of the S-matrix element, $\eta_L^2=|S_L|^2$). The boundary condition in this model is that the wave function consists of only ingoing waves at the strong absorption radius. In this way the final solution is independent of the nature of the real interaction in the strong absorption region.

The expression for η_L that is obtained within the barrier top or inverted parabola model is

$$\eta_L=|S_L|=\sqrt{R_L}=(1+e^{2\pi\alpha})^{-1/2}, \tag{1}$$

where

$$\alpha=\alpha(E,L)=[L-L_{\rm orb}(E)]/\Gamma(L)\ . \tag{2}$$

The functions $L_{\rm orb}(E)$ and $\Gamma(L)$ are obtained from the real potential. If $V_B(L)$ is the value of the total potential $V_{\rm tot}(L)$ at the top of the barrier for a given value of the angular momentum, then the orbiting angular momentum $L_{\rm orb}$ for a given center of mass bombarding energy E is defined by the relation $V_B[L_{\rm orb}(E)]=E$. Thus, $L_{\rm orb}$ is that value of the angular momentum for which the bombarding energy will just be sufficient to bring the particles to the top of the barrier in the total radial potential of relative motion. Classically, in that situation the particles have no radial velocity and so will orbit about each other at fixed separation. We note that $L_{\rm orb}$ is not, in general, an integer, and when considered as a function of $L_{\rm orb}$, V_B describes an elastic rotational band or trajectory.

The width $\Gamma(L)$ is related to the sum of Coulomb and nuclear potentials, which we denote by $V(R)$, through the relation

$$\Gamma(L)=\left[-\frac{V''R}{V'}\bigg|_{R=R_B}-3\right]^{1/2}. \tag{3}$$

The primes in Eq. (3) indicate differentiation with respect to R, and R_B is the radius at which the total potential $V_{\rm tot}(L)$ has its local maximum.

The prescription for calculating $\eta_L(E)$ is summarized for completeness. We first find the radius R_B at which the total potential

$$V_{\rm tot}=V_{\rm nuc}+V_{\rm Coul}+\frac{\hbar^2L_{\rm orb}(L_{\rm orb}+1)}{2}2\mu R^2 \tag{4}$$

has a local maximum (V_B) as a function of the variable $L_{\rm orb}$. The relation $V_B(L_{\rm orb})=E$ can then be inverted to give $L_{\rm orb}(E)$. Finally, at $R=R_B$ we also evaluate the potential $V(R)=V_{\rm nuc}+V_{\rm Coul}$ and its first and second derivatives. This determines $\Gamma(L)$ so that $\eta_L(E)$ can be calculated.

We have found that for nuclear potentials of the Woods-Saxon form, $L_{\rm orb}(E)$ and $\Gamma(L)$ can be represented by the following functions:

$$L_{\rm orb}(E)=\left[(E-E_0)\Big/\frac{\hbar^2}{2I}\right]^{1/2}-1/2 \tag{5}$$

and

$$\Gamma(L)=\Gamma_0+\frac{\gamma}{L+1} . \quad (6)$$

The parameters E_0, L, and γ are determined by specifying the parameters of the real Woods-Saxon potential (V_0, r_{0r}, and a_r) and carrying out the procedure described above. In physical terms, E_0 is the Coulomb barrier energy, I is an effective rigid body moment of inertia of the rotating system, and Γ is inversely proportional to the collision time. We note also that in the barrier top model L_{orb} and Γ are interpreted as specifying the position of the dominant pole in the complex L plane, $l=L_{\text{orb}}+i\Gamma/2$, for a given scattering energy.

The optical model parameter set that best describes the $^{13}C+^{13}C$ elastic scattering data ($V_0=16.0$, $r_{0r}=1.35$, $a_r=0.45$) yields these barrier top parameters:

$$E_0=6.0 \text{ MeV} , \quad \frac{\hbar^2}{2I}=E_L=0.063 \text{ MeV} ,$$

$$\Gamma_0=0.0 , \quad \gamma=44.0 .$$

We have calculated the elastic scattering using η_L from Eqs. (1)—(6) and the parameters listed above. For the nuclear phase shift δ_L ($S_L=\eta_L e^{2i\delta_L}$), we have used the parametrization

$$\delta_L=4\eta_L(1-\eta_L)(\delta_0+\delta_L'\times L) .$$

The values of the parameters $\delta_0(-7.5°)$ and $\delta_L'(1.5°)$ were chosen to provide a small and slowly varying real phase similar to that observed in the optical model calculations.

The calculations show that the values of the band parameters E_0 and E_L given above reproduce the positions of the structure in the excitation functions quite well. However, we find that the model incorrectly predicts the behavior of $\Gamma(L)$. The rather large value of Γ for small L results is an underestimation of the cross section just above the Coulomb barrier energy, while the rather small value of Γ for large L results in an overestimation at higher energies. A possible reason for this failure is that the actual potential barrier is not parabolic in shape. For small L, for example, the barrier is much wider than is determined by evaluating the second derivative at the top of the barrier. The actual barrier is also quite asymmetric in typical optical potentials. Thus, the effective width of the barrier should be increased for small L which results in a reduction of the corresponding L width, i.e., Γ becomes smaller. In fact, we have found that a better description of the experimental data is obtained if we choose $\Gamma_0=3.0$ and $\gamma=0.0$. This is consistent with the observation of Friedman and Goebel[23] that the displacement of the pole off the real axis in the complex L plane is approximately constant as a function of energy in optical model calculations.

The elastic scattering excitation functions calculated using the barrier top model with $\Gamma(L)=$const are presented and compared to experiment in Fig. 9. The agreement is comparable to the relatively good results obtained with the optical model. The slope of the departure from pure Coulomb scattering and the average cross section above the barrier are also well described. From the quality of the agreement of the barrier top model with experiment we conclude that the oscillations seen in the excitation function are consistent with the notion of orbiting. In other words, the gross structure oscillations arise from the interplay between strong absorption at small radii and surface transparency at the barrier.

IV. THE $^{13}C+^{13}C\rightarrow^{12}C+^{14}C$ NEUTRON TRANSFER REACTION

A. Introduction

To evaluate the extent to which a single step process is able to represent our global transfer data, we have carried out DWBA analyses of the $^{13}C+^{13}C\rightarrow^{12}C+^{14}C$ reaction using the optical potentials deduced above. Correspondingly detailed theoretical energy-angle differential cross sections using single particle MO models are not yet available. However, a number of general observations and conclusions concerning the failure of the DWBA and applicability of MO models are discussed. We consider a two-pole model for the transfer amplitude to analyze the transfer data for contributions from multistep processes. The analysis demonstrates that modifications of the S matrix qualitatively characteristic of MO effects are required to reproduce the salient features of the data satisfactorily. In addition, we report the results of extensive dynamic two-center shell model calculations that were carried out for the transfer reaction by Konnecke *et al.*[24] They have attained qualitative reproduction of our experimental data and their calculations provide a quantitative measure of the degree of adiabaticity required to obtain good agreement with experiment.

B. DWBA calculations

The radial integrals for the DWBA transfer amplitude were calculated using the code PTOLEMY.[25] Since a single step process for the $^{13}C+^{13}C\rightarrow^{12}C+^{14}C$ reaction effectively selects the $1p_{1/2}$ parentage, we have restricted the transferred neutron to the $1p_{1/2}$ shell model orbital for the DWBA calculations. In this case the allowed 1 transfers are $\Delta l=0$ (normal) and $\Delta l=1$ (recoil). These correspond to changes in channel spin of 0 and 1, respectively. The spectroscopic factors were taken from the calculations of Cohen and Kurath.[26] The potential well for which the neutron bound state wave functions were calculated had radius $R=r_0A^{1/3}$, with $r_0=1.25$ fm, and diffuseness $a=0.65$ fm. The $^{13}C+^{13}C$ Woods-Saxon optical model parameters listed in Table I were used for the calculation of both the entrance and exit channel distorted waves.

To compare with experiment and to study the energy dependence of the DWBA prediction, the PTOLEMY calculations were carried out for 31 energies in the range $6.0\leq E_{\text{c.m.}}(^{13}C+^{13}C)\leq 36.0$ MeV. Properly symmetrized cross sections were obtained by including the direct and dominant exchange terms in the transfer amplitude. The exchange terms that are most important are discussed by several authors.[27] We have followed their precedent and have included the terms which are analogous to those included in typical elastic exchange calculations. When the dominant exchange terms are included, proper symmetrization of the $^{13}C+^{13}C\rightarrow^{12}C+^{14}C$ amplitude requires replacing the unsymmetrized amplitudes $f^{\Delta l=0}(\theta,\phi)$ and $f^{\Delta l=1}(\theta,\phi)$ by

$$\frac{1}{\sqrt{2}}[f^{\Delta l=0}(\theta,\phi)+f^{\Delta l=0}(\pi-\theta,\phi+\pi)]$$

and

$$\frac{1}{\sqrt{2}}[f^{\Delta l=1}(\theta,\phi)-f^{\Delta l=1}(\pi-\theta,\phi+\pi)]\ ,$$

respectively.

In terms of a partial wave decomposition of the transfer amplitude, the antisymmetrization requirement together with angular momentum and parity conservation force the change in channel spin S, orbital angular momentum transfer 1, and change in channel spin magnetic substate projection m to be identically equal. In addition, the relative orbital angular momentum L is conserved, i.e., the orbital angular momentum of the exit channel is necessarily that of the entrance channel. Finally, the terms of the decomposition corresponding to even partial waves contribute only to the $\Delta l=\Delta S=\Delta m=0$ transition, while those corresponding to the odd partial waves contribute only to the $\Delta l=\Delta S=\Delta m=1$ transfer.

After we make use of the properties of the spherical harmonics, the DWBA cross section for the $^{13}C+^{13}C\rightarrow{}^{12}C+^{14}C$ reaction is given as

$$\frac{d\sigma}{d\Omega}(\theta)=\frac{10}{E_iE_f}\frac{k_f\pi}{k_i 3}S_iS_f\left\{\left|\sqrt{2}\sum_{L(\text{even})}I^0_{L,L}Y^0_L(\theta)\right|^2+2\left|\sqrt{2}\sum_{L(\text{odd})}I^1_{L,L}Y^1_L(\theta)\right|^2\right\}. \tag{7}$$

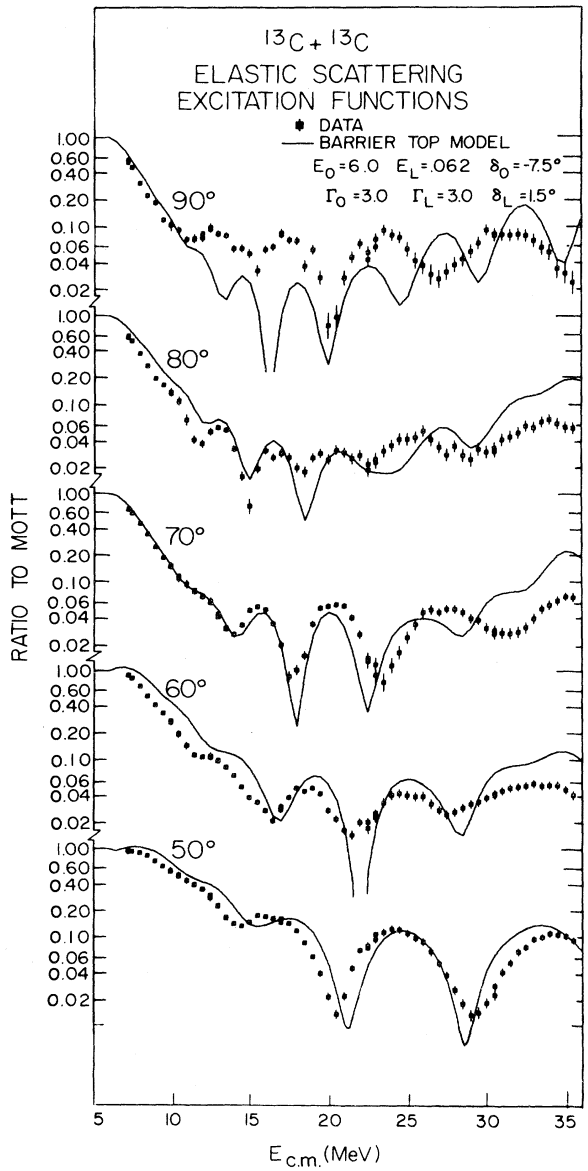

FIG. 9. Barrier top model calculations for $^{13}C+^{13}C$ elastic excitation functions.

In the above equation, $I^{\Delta l}_{L_i,L_f}$ is the radial integral calculated by PTOLEMY, E_i and E_f are the c.m. energies in the entrance and exit channels, respectively, and k_i and k_f are the corresponding wave numbers. The factor S_iS_f denotes the product of the spectroscopic factors and is calculated by Cohen and Kurath to be $S_iS_f\approx 1.06$.

We begin the discussion of the comparison of the DWBA with experiment by considering the angular distributions at a single energy, $E_{c.m.}=17.5$ MeV. In the lower portion of Fig. 10 the individual components of the DWBA angular distribution, $\Delta l=0$ and $\Delta l=1$, are plotted together with their sum. As can be seen, the two components are of approximately equal magnitude and for $30°<\theta_{c.m.}<60°$ are roughly out of phase. This results in a rather smooth DWBA differential cross section. In contrast, the experimental angular distribution, displayed as a solid line in the upper portion of Fig. 8, shows evidence of strong oscillations in this angular region.

If one of the 1-transfer contributions to the theoretical cross section were to be enhanced relative to the other, the calculated differential cross section would have oscillations. The discrepancy between the calculation and experiment may therefore be a result of the failure of the DWBA to predict the correct ratio of the two strengths. It is possible for models in which multistep processes are important to predict angular momentum transfer strengths that are significantly different from the DWBA values. For example, a qualitative model of MO behavior[28] predicts the ratio of $\Delta l=1$ to $\Delta l=0$ transition strengths to be smaller than the corresponding DWBA value. This is because the entrance channel ($^{13}C+^{13}C$) states of channel spin $S=1$ are forbidden from mixing with the exit channel ($^{12}C+^{14}C$) states of channel spin $S=0$, and thus the $\Delta l=\Delta S=1$ transition occurs only via recoil effects. Multistep processes can mix the states contributing to the $\Delta l=\Delta S=0$ transition, however. In particular, a molecular distortion of the valence neutron wave function enhancing the probability of finding the neutrons near the line joining the cores (corresponding to a $\Delta l=0$ transfer) or a molecular shift of the valence neutron energy levels would enhance the probability of the $\Delta l=\Delta S=0$ component. We note, for example, that the asymptotic $^{13}C+^{13}C$ and $^{12}C+^{14}C$ ground state configurations in the linear-combination-of-nuclear-orbitals model,[29] that have channel spin $S=0$ and contribute to the $\Delta S=0$

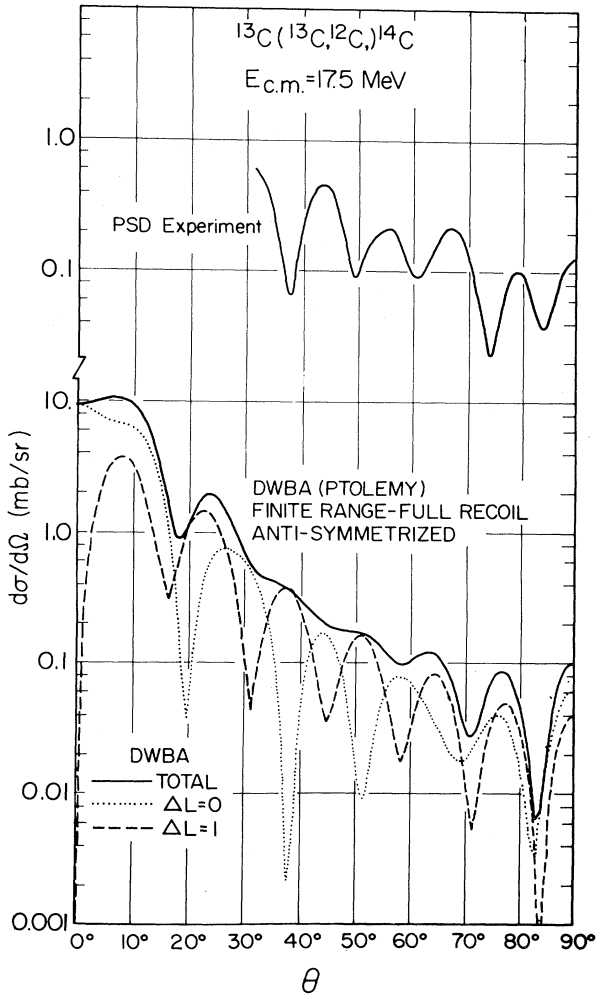

FIG. 10. Comparison of the DWBA transfer calculation to experiment at $E_{c.m.}=17.5$ MeV.

transfer, are degenerate in the limit $R\rightarrow 0$ if the reaction occurs adiabatically.

It has not been possible to extract unambiguous values for the individual $\Delta l=0$ and $\Delta l=1$ contributions to our measured cross sections for direct comparison with theoretical models using a phase shift analysis. This is largely due to the fact that the contributing spherical harmonics are not orthogonal in the limited angular range $30°\leq\theta\leq 90°$. In addition to the present data, measurements in the interval $0°\leq\theta\leq 30°$ (with special emphasis on the very forward region, $\theta<1°$) are necessary to extract the separate $\Delta l=0$ and $\Delta l=1$ contributions in a model independent fashion. Although a quantitative ratio could not be determined, the data for all energies suggests that the $\Delta l=0$ transfer provides the dominant contribution in the energy range studied.

In Fig. 11 we compare the DWBA calculations to the experimental data over the entire energy region by considering energy-angle surface plots of the differential cross section. Again, we see that the DWBA predicts far too little structure in the 30° to 60° region. However, the $\Delta l=0$ and $\Delta l=1$ terms separately have the oscillatory behavior observed in the data. At the lower energies the DWBA, as well as multistep models, predicts the $\Delta l=0$ transfer to dominate because the nuclei remain spatially separated and thus finite-range and recoil effects are small. The failure of the DWBA at the lower energies must therefore reside in either the choice of interaction potentials or in the reaction mechanism itself.

At higher energies, the difference between the critical angular momenta of relative motion in the entrance and exit channels becomes relatively smaller. Thus, the phase and period of the angular oscillations are less sensitive to changes in the effective interaction and more sensitive to the 1 transfer. By examining the surface plots for the higher energy data we see that the $\Delta l=0$ contribution is more nearly in phase with experiment. In the region near 30°, for example, both the experiment and $\Delta l=0$ DWBA calculation show a ridge in the cross section surface. The $\Delta l=1$ DWBA calculations, however, show a valley in the same energy and angular region. Thus, to obtain better agreement with experiment it appears that the role of the $\Delta l=0$ transfer should be enhanced. We note that although a phase shift analysis of the present data was unable to fix a value for the $(\Delta l=1)/(\Delta l=0)$ ratio, adequate fits to the experimental data over the entire energy range could be obtained if a pure $\Delta l=0$ transfer was assumed.

It is an intriguing possibility that the discrepancies between the DWBA calculations and experiment are the manifestation of molecular orbital type multistep processes. Because of the qualitative nature of the MO predictions we cannot make a definitive statement. However, if MO effects are responsible for the discrepancies at the relatively low bombarding energies we have investigated, then the DWBA should become better at higher energies where the collision time is shorter. Measurements of the differential cross section for a reaction similar to the $^{13}C+^{13}C\rightarrow^{12}C+^{14}C$ reaction, but at significantly higher energy, have been made by Liu *et al.*[30] The reaction they studied was $^{12}C+^{13}C$ elastic scattering, but the measurements were carried out in an angular region where the cross section is dominated by the neutron transfer amplitude, i.e., the amplitude for $^{13}C(^{12}C,^{13}C)^{12}C$.

The data of Liu *et al.* are graphed in Fig. 12. The angular distribution is characteristically a smooth function of the scattering angle. Compared to the data is the DWBA calculation by DeVries.[31] This calculation shows that the incoherent addition of the $\Delta l=0$ and $\Delta l=1$ contributions, which are out of phase, is absolutely necessary to reproduce the experimental observations at $E_{c.m.}=45$ MeV. Hence, the highest energy neutron transfer data are adequately explained by a single-step mechanism (DWBA), but the low energy data presented here are not. The observation of dramatic oscillations in the $^{13}C+^{13}C\rightarrow^{12}C+^{14}C$ angular distributions at lower energy suggests that higher-order processes are important and, in particular, that the anomalies may be of MO origin.

Our attention so far has focused on the $^{13}C+^{13}C\rightarrow^{12}C+^{14}C$ angular distributions. For another comparison of the DWBA to experiment, we consider the energy dependence of the transfer cross section. Because the cross section at $\theta_{c.m.}=90°$ appears always to be a local maximum in the angular distribution, it is convenient to choose this angle for the comparison. The theoretical and experimental excitation functions are plotted in Fig. 13.

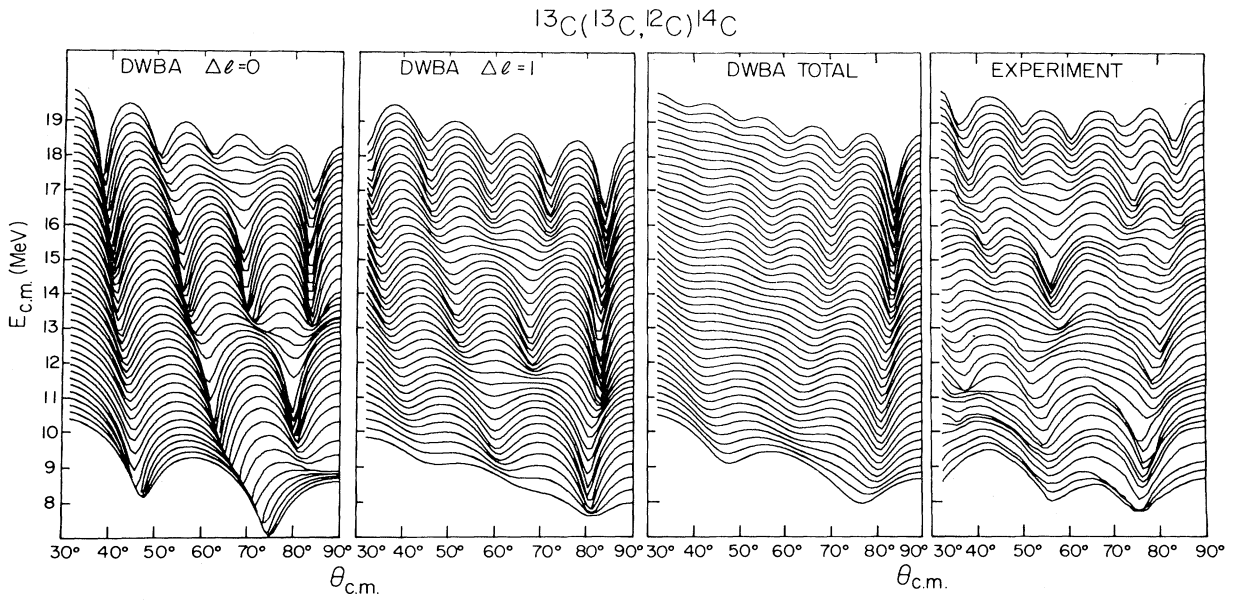

FIG. 11. Global features of the DWBA and experimental differential cross sections for the $^{13}C+^{13}C\rightarrow{}^{12}C+^{14}C$ reaction.

Like the data, the DWBA excitation function shows evidence for oscillations. This can be attributed to our optical potential, which incorporates the gross structure oscillations observed in the elastic scattering of $^{13}C+^{13}C$. Although the DWBA does predict oscillations, it fails to reproduce the general energy dependence of the experimental cross section. Experiment shows that the cross section at the peaks of the oscillations remains relatively constant over a wide energy range. The DWBA, however, predicts a cross section which generally decreases with increasing bombarding energy. This discrepancy is considered significant, and in the following subsection we

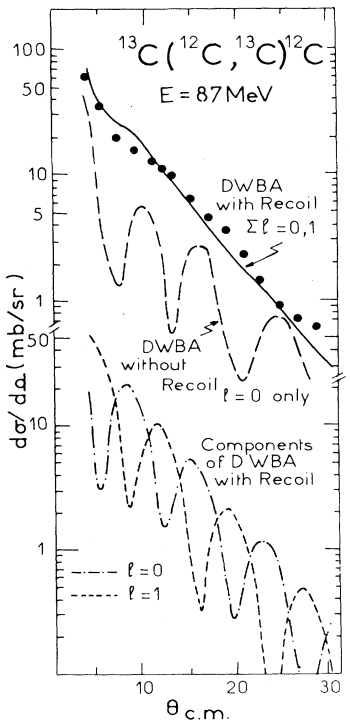

FIG. 12. Behavior of neutron transfer at higher energy. The measurements are those of Liu *et al.* (Ref. 30) and the DWBA analysis was carried out by DeVries (Ref. 31).

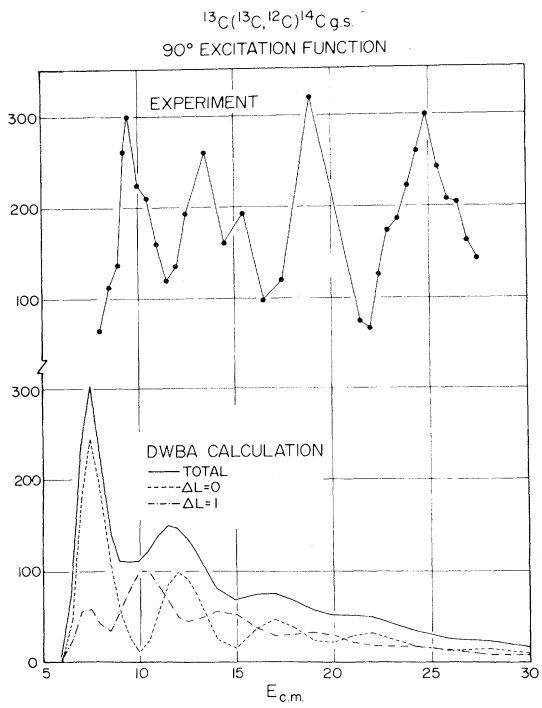

FIG. 13. DWBA and experimental 90° excitation function for the $^{13}C+^{13}C\rightarrow{}^{12}C+^{14}C$ transfer reaction. (Energy in units of MeV.)

show that it can be interpreted as evidence for molecular orbital effects.

C. Two pole model

It has been suggested by Carlson and McVoy[32] that the occurrence of multistep processes in a heavy-ion transfer reaction can be evaluated using a two-pole or two-pole—one-zero parametrization of the S matrix. The idea is based on two findings. One is the observation of Fuller and McVoy[33] and Friedman and Goebel[23] that the DWBA amplitude for typical heavy-ion reactions is dominated by two-poles which are associated with the grazing partial waves in the entrance and the exit channels. The other is their finding[32] that the L dependence of the S matrix for coupled-channel Born-approximation (CCBA) transfer calculations that have large multistep contributions is often characterized by either a shift in the poles from the positions determined by the entrance and exit channel elastic scattering, or a prominent dip (characteristic of a zero) believed to be caused by the interference of the amplitudes corresponding to different multistep routes. Because of the success of the barrier top (one-pole) model in reproducing the $^{13}C+^{13}C$ elastic scattering data, and because the position of the poles are related to the value of the potential at the barrier and to the intrinsic collision time, we have considered the two-pole model to look for evidence of MO effects in the $^{13}C+^{13}C\rightarrow^{12}C+^{14}C$ reaction.

As discussed previously, there is reason to believe that the $\Delta l=0$ component of the transfer dominates over the energy region of present interest. Taking this as a hypothesis, we have carried out two-pole calculations with only a $\Delta l=0$ term included. The expression used for the transfer S matrix is

$$S(l)=\frac{Ce^{i[\sigma_i(L)+\sigma_f(L)]}(L-L_B-iy)e^{-(L-L_B)^2/\Delta^2}}{(L-p_1)(L-p_2)} .$$

Because the model only predicts the L dependence of the transfer amplitude, the constant C sets the absolute cross section scale. The phase factor $e^{i[\sigma_i(L)+\sigma_f(L)]}$ accounts for the Coulomb phase shift in the entrance (i) and exit (f) channels. The purpose of the factor

$$(L-L_B-iy)\exp[-(L-L_B)^2/\Delta^2]$$

is to regulate the L^{-1} dependence of the pole contributions with the Gaussian factor, and to provide a smooth background phase with the zero factor. Although L_B, y, and Δ^2 are parameters of the model, Carlson and McVoy have found that the angular distributions are not very sensitive to the exact values. We have obtained good fits to the experimental data and the $\Delta l=0$ DWBA angular distributions for the $^{13}C+^{13}C\rightarrow^{12}C+^{14}C$ reaction by setting $y=4.0$, $\Delta^2=36$, and

$$L_B=[\mathrm{Re}(p_1)+\mathrm{Re}(p_2)]/2-10 .$$

To introduce systematics into the study of the energy dependence of the transfer cross section we did not consider the positions of the poles as explicit parameters. Rather we took

$$p_1(E)=L_{\mathrm{orb}}(E)+\frac{\Gamma}{2}i$$

and

$$p_2(E)=L_{\mathrm{orb}}(E+Q_G)+\frac{\Gamma}{2}i ,$$

where $L_{\mathrm{orb}}(E)$ and Γ are parametrized according to Eqs. (5) and (6), and E is the entrance channel c.m. bombarding energy. For the parameters that fix the trajectory of L_{orb} we took the values used for $^{13}C+^{13}C$ elastic scattering calculations, namely,

$$E_0=6.0$$

and

$$\frac{\hbar}{2I}=0.063 \text{ MeV} .$$

The only free parameters of the model are Q_G, which is interpreted as the Q value in the region of the barrier, and Γ, which is related to the collision time through

$$\frac{\hbar}{\Delta t}\sim\Delta E\propto\frac{(\hbar c)^2}{\mu c^2 R}L_{\mathrm{orb}}^2\Gamma .$$

If we set Q_G to the asymptotic Q value (3.23 MeV) and Γ to the value determined by the analysis of $^{13}C+^{13}C$ elastic scattering excitation functions ($\Gamma=3.0$), then we expect to obtain cross sections with features similar to the DWBA prediction. Figure 14 (bottom) shows the 90° excitation function calculated with the values of the parameters specified above and $C^2=0.18$. As with the DWBA calculation, Fig. 13, the two-pole calculation with these parameters shows a large cross section near threshold which rapidly decreases as the bombarding energy is increased. The excitation functions also show mild oscillations, although the maxima do not occur at exactly the same energies as those of the DWBA.

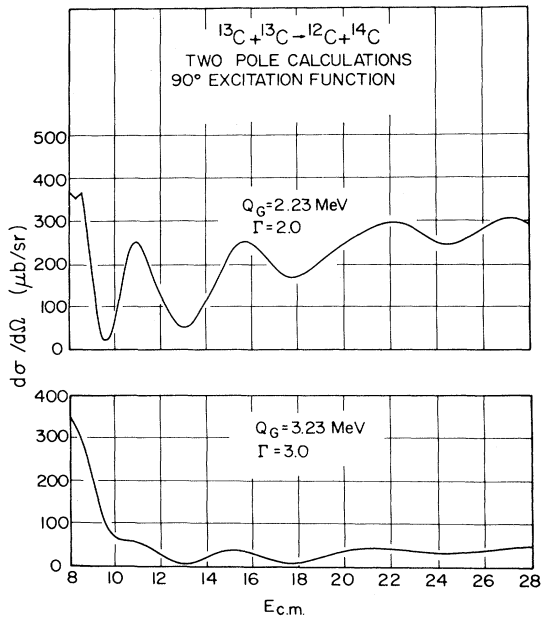

FIG. 14. 90° transfer excitation functions calculated using the two-pole model. The pole trajectories are specified by a simplifying parametrization, as described in the text.

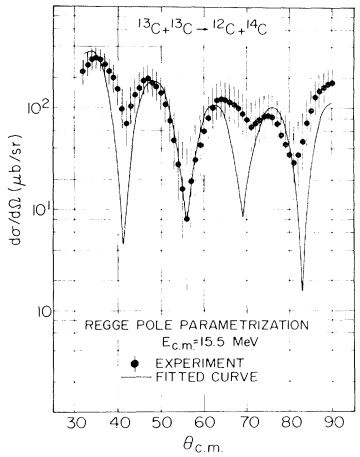

FIG. 15. Pole model comparison to smoothed experimental angular distribution. The range of experimental uncertainty is indicated by artificial error bars.

In preliminary attempts to improve the agreement of the two-pole model calculations with experiment, it was found necessary to reduce the separation between the poles and to move them closer to the real axis. These shifts in the positions of the poles correspond to a reduction of the Q value in the region of the barrier and an increase in the collision delay time. Figure 14 (top) shows the results of the two-pole calculation when the Q value in the region of the barrier is reduced by 1 MeV to $Q_G=2.23$ MeV and the L width is decreased by a factor of $\frac{2}{3}$ to $\Gamma=2.0$, corresponding to a 50% increase in the collision time. These values provide the best reproduction of the experimental angular distribution at a representative energy $E_{c.m.}=15.5$ MeV, Fig. 15. The value of the normalization constant was slightly reduced to $C^2=0.14$ to scale the cross section for the lowest energy calculated (8 MeV) to roughly that of the corresponding point of the excitation function in the bottom portion of Fig. 14.

We note how these basic changes in Q_G and Γ dramatically enhance the 90° cross section at the higher energies. In particular, the excitation function oscillates strongly and the peak cross sections are nearly constant over the wide energy range studied—in qualitative agreement with the experiment. The calculated peak cross section does increase gradually with increasing bombarding energy, suggesting that the actual reduction in the Q value decreases with energy. This is to be expected if multistep processes such as MO effects are important at the lower energies and the likelihood that the reaction proceeds as a single-step process increases as the collision time is reduced.

To summarize, we note that the enhanced magnitude, and not the oscillations, of the experimental 90° excitation function appears to be the significant feature of the data. To improve the agreement of the two-pole model calculations with experiment it is necessary to reduce the separation of the poles from approximately $1.5\hbar$ to approximately $0.8\hbar$ and to move the poles closer to the real axis. These effects reduce the innate destructive interference of the even partial wave spherical harmonics at 90° that differ by two units of angular momentum; see Eq. (7) and note

$$Y^0_{L=\text{even}}\ (\theta=90°)\simeq(-)^{L/2}\frac{1.123}{\sqrt{4\pi}}\ .$$

This diminished interference causes a general increase in the cross section at the backward angle region, i.e., near 90°. The analysis of the data shows strong evidence for the occurrence of significant multistep contributions. We cannot prove that the required shifts in the positions of the poles are of molecular orbital origin, but the relationship between the positions of the poles along the real axis and the values of the potentials at the barriers in the entrance and exit channels naturally suggests that the shifts may arise from changes in the internal energy of the system of valence particles. Likewise, the trend toward smaller Γ can be interpreted as an indication that the two valence neutrons become more bound when the two nuclei are in proximity.

D. Dynamic two-center shell model

Konnecke *et al.*[24] have recently completed an extensive numerical dynamic two-center shell model (DTCSM) calculation for the single neutron transfer process in the specific case of the $^{13}C+^{13}C\rightarrow^{12}C+^{14}C$ reaction. The model, which is molecular orbital in spirit, describes the excitable ^{12}C cores via a collective rotator-vibrator formalism and the valence neutrons via TCSM wave functions. Transfer and excitation of the valence neutrons is assumed to result from the dynamic radial and rotational couplings. Of particular significance in their approach is the inclusion of the static polarization effects on the two-center wave functions and the dynamic polarization of the valence particle wave functions as a consequence of the proximity of the nuclear cores during the collision.

The optical model parameters used by Konnecke *et al.* are those of the shallow potential we have found to describe our elastic scattering data. They also assume that the ^{13}C ground state is adequately represented as a $1p_{1/2}$ valence neutron coupled to an unexcited ^{12}C core. The detailed and complex model calculations explicitly incorporate the required antisymmetrization of the extra core neutrons in addition to the symmetrization of the cores. In all, some 29 coupled channels were included in Konnecke's calculations, and we refer the reader to his work[34] for details.

In Fig. 16 we show the comparison of typical results of Konnecke's calculations with our data for the $^{13}C+^{13}C$ elastic 90° excitation function and the $^{13}C+^{13}C\rightarrow^{12}C+^{14}C$ transfer angular distributions measured at $E_{c.m.}=10.0$ and 15.5 MeV. The parameter ϵ denotes the degree of adiabaticity of the assumed interaction with $\epsilon=1$ representing the sudden limit and $\epsilon=0$ the strictly adiabatic case. In general, $\epsilon=0.65$ provides the best overall qualitative reproduction of the experimental data. As is evident in this figure, the model transfer cross section magnitudes are particularly sensitive to the adiabaticity parameter. The figure also illustrates that the molecular orbital model as implemented by Konnecke *et al.* succeeds in reproducing the dominant structure of our data. These results provide additional evidence that neutron transfer in the $^{13}C+^{13}C$ system is dominated by a molecular orbital rather than a direct (DWBA) mechanism.

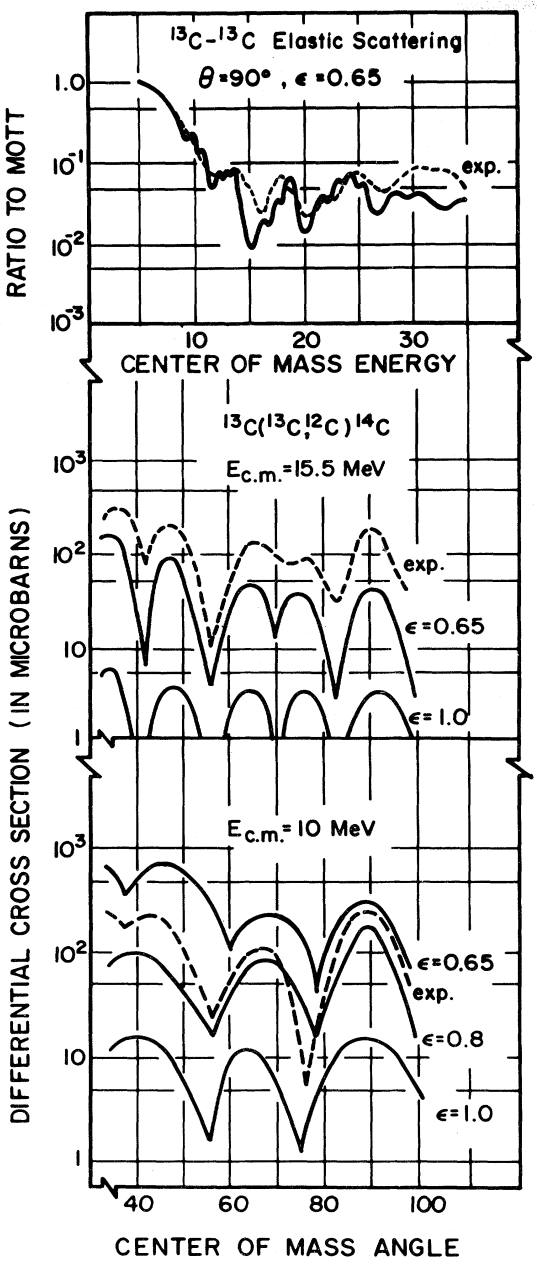

FIG. 16. Comparison of dynamic two-center shell model calculations of Konnecke *et al.* (Ref. 34) to selected transfer angular distributions.

V. SUMMARY AND CONCLUSIONS

We have reported a detailed study of the angle and energy dependence of the cross section for $^{13}C+^{13}C$ elastic scattering and for the $^{13}C+^{13}C\rightarrow^{12}C+^{14}C$ single neutron transfer reaction as part of a systematic search for single-particle molecular orbital effects in nuclear systems.

We find that our elastic scattering data are adequately described using the optical model, and that the optimum Woods-Saxon parameters are similar to those used to describe other systems in this mass region, such as $^{16}O+^{16}O$. We have shown that the barrier top model also describes the experiment and that it provides a physical interpretation of the $^{13}C+^{13}C$ gross structure in terms of orbiting. These findings suggest that the elastic scattering is dominated by geometrical effects and that there is no evidence for strong elastic exchange processes. The results also support our contention that the same optical model parameter set can be applied with confidence to $^{12}C+^{14}C$ elastic scattering.

Distorted-wave Born approximation calculations were unable to reproduce the salient features of our transfer data, either in terms of the oscillations in the angular distributions or in the magnitude and structure of the excitation functions. The data appear to be characterized by a larger ratio of the $\Delta l=0$ to $\Delta l=1$ orbital angular momentum transfer contributions. Polarization of the neutron orbits and/or a shift in their single particle energy would favor such an increase. We used two-pole model calculations to analyze the transfer data for multistep contributions. An observed displacement in the pole positions compared to those expected for a single step process suggests a significant increase in the collision interaction time and a shift in the single particle energy of the neutron levels during the collision. Sophisticated dynamic two-center shell model calculations carried out by Konnecke *et al.* for our transfer data succeed in reproducing the main features of the experiment. With the adiabaticity of the reaction an adjustable parameter, they show that the sudden approximation fails to describe the data and that the best agreement obtained includes significant multistep contributions corresponding to single particle nuclear molecular behavior.

From our study we conclude that the motion of the valence neutrons in the $^{13}C+^{13}C\rightarrow^{12}C+^{14}C$ reaction are strongly and simultaneously influenced by both cores during the transfer process. This behavior is characteristic of a molecular (single-particle) rather than a direct (DWBA) mechanism, and our results present evidence that the single-particle analog of atomic molecular motion plays an important role in nuclear rearrangement reactions in this mass region.

ACKNOWLEDGMENTS

We are grateful to R. Konnecke, W. Scheid, and W. Greiner for having made the results of their theoretical calculations available prior to publication. This work was supported by U. S. Department of Energy Contract No. EY-76-C-02-3074.

*Present address: Bell Laboratories, Holmdel, NJ 07733.
†Present address: Oak Ridge National Laboratory, Oak Ridge, TN 37830.
‡Present address: King Faisal Specialist Hospital and Research Centre, P.O. Box 3354, Riyadh, Saudia Arabia.
§Present address: 3M Company, St. Paul, MN 55144.

[1]P. D. Bond, C. Chasman, J. D. Garrett, C. K. Gelbke, O. Hanson, M. J. Levine, A. Z. Schwarzschild, and C. E. Thorn, Phys. Rev. Lett. 36, 300 (1976).
[2]W. Henning, Y. Eisen, J. R. Erskine, D. G. Kovar, and B. Zeidman, Phys. Rev. C 15, 292 (1977).
[3]P. D. Bond, M. J. Levine, D. J. Pisano, C. E. Thorn, and L. L. Lee, Jr., Phys. Rev. C 19, 2160 (1979).
[4]S. J. Sanders, M. Paul, J. Cseh, D. F. Gessaman, W. Henning, D. G. Kovar, R. Kozub, C. Olmer, and J. P. Schiffer, Phys. Rev. C 21, 1810 (1980).
[5]K. Pruess, Nucl. Phys. A278, 124 (1977); K. Pruess and P. Lichtner, *ibid.* A291, 475 (1977).
[6]E. A. Seglie and R. J. Ascuitto, Phys. Rev. Lett. 39, 688 (1977).
[7]E. A. Seglie, J. F. Petersen, and R. J. Ascuitto, Phys. Rev. Lett. 42, 956 (1979).
[8]J. Y. Park, W. Scheid, and W. Greiner, Phys. Rev. C 20, 188 (1979).
[9]B. Imanishi and W. von Oertzen, Phys. Lett. 87B, 188 (1979).
[10]W. von Oertzen, B. Imanishi, H. G. Bohlen, W. Treu, and H. Voit, Phys. Lett. 93B, 21 (1980).
[11]S. K. Korotky, K. A. Erb, S. J. Willett, and D. A. Bromley, in *Proceedings of the International Conference on Nuclear Physics,* edited by R. M. Diamond and J. O. Rasmusen (University of California, Berkeley, California, 1980), Vol. 1, p. 549; S. K. Korotky, K. A. Erb, R. L. Phillips, S. J. Willett, and D. A. Bromley, *ibid.*, p. 544.
[12]D. A. Bromley, M. M. Hindi, K. A. Erb, S. K. Korotky, and S. J. Willett (unpublished).
[13]H. D. Helb, P. Duck, G. Hartmann, G. Ischenko, F. Siller, and H. Voit, Nucl. Phys. A206, 385 (1973).
[14]W. Reilly, R. Wieland, A. Gobbi, M. W. Sachs, J. V. Maher, D. Mingay, R. H. Siemssen, and D. A. Bromley, in *Proceedings of the International Conference on Nuclear Reactions Induced by Heavy Ions, Heidelberg, 1969,* edited by R. Bock and W. R. Hering (North-Holland, Amsterdam, 1970), p. 93.
[15]W. Reilly, R. Wieland, A. Gobbi, M. W. Sachs, and D. A. Bromley, Ref. 14, p. 95.
[16]J. V. Maher, M. W. Sachs, R. H. Siemssen, A. Weidinger, and D. A. Bromley, Phys. Rev. 188, 1665 (1969).
[17]H. G. Bohlen, M. Feil, A. Gamp. B. Kohlmeyer, N. Marquardt, and W. von Oertzen, Phys. Lett. 41B, 425 (1972).
[18]L. T. Chua, A. Gobbi, M. W. Sachs, D. Shapira, R. Weiland, and D. A. Bromley, Nuovo Cimento 47A, 443 (1978).
[19]K. A. Erb, R. R. Betts, S. K. Korotky, M. M. Hindi, P. P. Tung, M. W. Sachs, S. J. Willett, and D. A. Bromley, Phys. Rev. C 22, 507 (1980).
[20]E. H. Auerbach, Comput. Phys. Commun. 15, 165 (1978).
[21](a) R. H. Siemssen, H. T. Fortune, A. Richter, and J. W. Tippie, Phys. Rev. C 5, 1839 (1972); (b) A. Gobbi, R. Wieland, L. Chua, D. Shapira, and D. A. Bromley, *ibid.* 7, 30 (1973).
[22]K. W. Ford, D. L. Hill, M. Wakano, and J. A. Wheeler, Ann. Phys. (N.Y.) 7, 239 (1959).
[23]W. A. Friedman and C. J. Goebel, Ann. Phys. (N.Y.) 104, 145 (1977).
[24]R. Konnecke, W. Scheid, and W. Greiner (unpublished); private communication to D. A. Bromley.
[25]D. H. Gloeckner,* M. H. Macfarlane, and S. C. Pieper, Argonne National Laboratory Report No. ANL-76-11, 1976 (unpublished); Revision No. 1, 1978 (unpublished).
[26]S. Cohen and D. Kurath, Nucl. Phys. A101, 1 (1967).
[27]G. Breit, J. A. Polak, and D. A. Torcha, Phys. Rev. 161, 993 (1967); P. J. A. Buttle and L. J. B. Goldfarb, Nucl. Phys. 78, 409 (1966); P. Braun-Munzinger, A. Gamp, C. K. Gelbke, and H. L. Harney, Z. Phys. A 276, 107 (1976); M. LeMere and Y. C. Tang, Phys. Rev. C 19, 391 (1979).
[28]S. K. Korotky, doctoral dissertation, Yale University, 1980 (unpublished).
[29]W. von Oertzen and H. G. Bohlen, Phys. Rep. 19C, 1 (1975).
[30]M. Liu, W. von Oertzen, J. C. Jacmart, F. Pougheon, M. Riou, J. C. Roynette, and C. Stephen, Nucl. Phys. A165, 118 (1971).
[31]R. M. DeVries, Phys. Rev. C 8, 951 (1973).
[32]B. V. Carlson and K. W. McVoy, Nucl. Phys. A292, 310 (1977).
[33]R. C. Fuller and K. W. McVoy, Phys. Lett. 55B, 121 (1975).
[34]R. Konnecke, doctoral dissertation, Institute fur Theoretische Physik, 1982 (unpublished).